

# Perspectives on epitaxial InGaP for quantum and nonlinear optics

Joshua Akin,<sup>1,2,\*</sup> Yunlei Zhao,<sup>1,2,\*</sup> A. K. M. Naziul Haque,<sup>1,2</sup> and Kejie Fang<sup>1,2,†</sup>

<sup>1</sup>*Holonyak Micro and Nanotechnology Laboratory and Department of Electrical and Computer Engineering, University of Illinois at Urbana-Champaign, Urbana, IL 61801 USA*

<sup>2</sup>*Illinois Quantum Information Science and Technology Center, University of Illinois at Urbana-Champaign, Urbana, IL 61801 USA*

Nonlinear optical materials are essential for the development of both nonlinear and quantum optics and have advanced recently from bulk crystals to integrated material platforms. In this Perspective, we provide an overview of the emerging InGaP  $\chi^{(2)}$  nonlinear integrated photonics platform and its experimental achievements. With its exceptional  $\chi^{(2)}$  nonlinearity and low optical losses, the epitaxial InGaP platform significantly enhances a wide range of second-order nonlinear optical effects, from second-harmonic generation to entangled photon pair sources, achieving efficiencies several orders of magnitude beyond the current state of the art. Moreover, the InGaP platform enables quantum nonlinear optics at the few- and single-photon levels via passive nonlinearities, which has broad implications for quantum information processing and quantum networking. We also examine the current limitations of the InGaP platform and propose potential solutions to fully unlock its capabilities.

## I. INTRODUCTION

Nonlinear optical materials play a pivotal role in advancing both nonlinear optics and quantum optics. In addition to their classical uses, such as in optical parametric oscillators [1] and high-harmonic generation [2, 3], nonlinear crystals have long been employed to generate quantum light, including entangled photon pairs [4] and squeezed light [5]. These quantum light sources are foundational to the experimental progress in quantum communications [6], quantum sensing [7], and quantum computing [8].

In recent years, nonlinear optical materials have progressed from bulk crystals to integrated material platforms, driven by advances in material growth and fabrication techniques. These developments have facilitated the use of materials with higher nonlinear susceptibilities and the creation of light-confining nanophotonic structures, resulting in a substantial increase in nonlinear optical efficiencies [9]. Fig. 1 summarizes several leading second-order ( $\chi^{(2)}$ ) nonlinear thin-film materials, including their second-order susceptibility and transparency window. Among them, III-V materials, including  $\text{Al}_x\text{Ga}_{1-x}\text{As}$  and  $\text{In}_{0.5}\text{Ga}_{0.5}\text{P}$  (InGaP), exhibit the highest  $\chi^{(2)}$  susceptibilities and a broad transparency window. They can be epitaxially grown on the GaAs substrate, leading to versatile III-V integrated photonics platforms. In the case of  $\text{Al}_x\text{Ga}_{1-x}\text{As}$ , increasing the aluminum composition expands the bandgap, but this also results in a marked decrease in the second-order susceptibility [10]. Moreover, arsenic-based III-V materials suffer from strong optical absorption at wavelengths below 800 nm [11, 12], due to the antibonding As-As surface state that lies below the bandgap [13]. These limitations have

made  $\text{Al}_x\text{Ga}_{1-x}\text{As}$  a less suitable choice for second-order nonlinear optics involving light in the telecommunication band and the corresponding second harmonics.

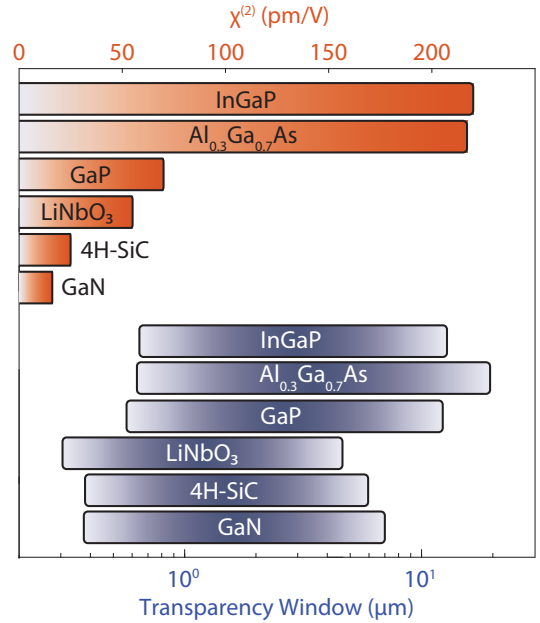


FIG. 1.  $\chi^{(2)}$  susceptibility and transparency window of leading thin-film second-order nonlinear materials.

In this Perspective, we provide an overview of the emerging InGaP  $\chi^{(2)}$  nonlinear integrated photonics platform and discuss its unique advantages for nonlinear and quantum optics involving the telecommunication band. In Sec. II we discuss the material properties of InGaP. Section III discusses properties of InGaP nonlinear photonic devices, including microring resonators and waveguides. Sections IV and V discuss nonlinear and quantum optical effects of the cavity and waveguide, respectively. Finally, we briefly examine the current limitations of the

\* These authors contributed equally to this work.

† kfang3@illinois.edu

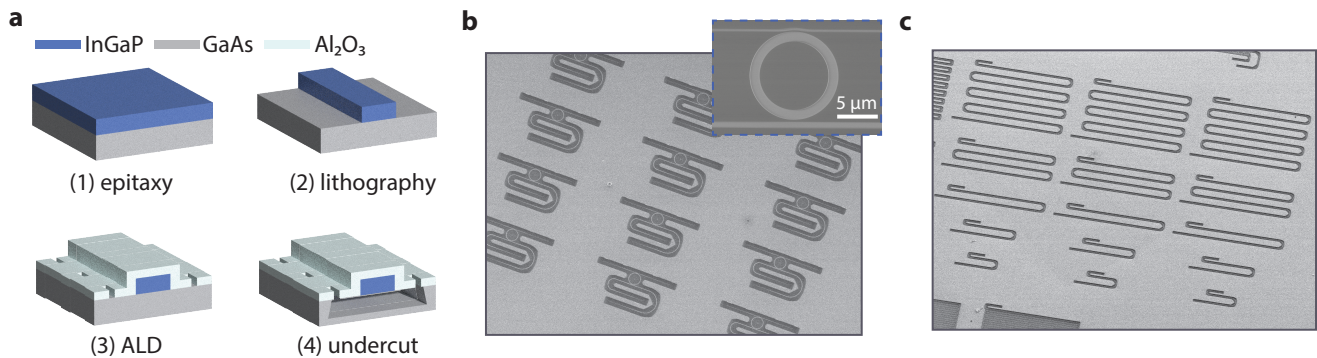


FIG. 2. **a.** Illustration of the fabrication process of the suspended InGaP photonic integrated circuit. **b.** SEM images of waveguide-coupled microring resonators. **c.** SEM image of waveguide devices.

InGaP platform and propose potential solutions.

## II. INGAP AS A PRIME NONLINEAR MATERIAL

InGaP is a III-V semiconductor material that is lattice-matched to GaAs. As a result, thin-film single-crystalline InGaP can be epitaxially grown on the GaAs substrate via metal-organic chemical vapor deposition (MOCVD) or molecular beam epitaxy (MBE). Due to its high electron mobility, direct bandgap and thermal stability, InGaP has been used for applications including solar cells [14], LEDs [15], photon detectors [16], heterojunction bipolar transistors [17] and high-electron-mobility transistors [18]. In addition, thin-film InGaP has also been studied for nonlinear optics by exploiting its large Kerr nonlinearity [19, 20], leading to the demonstration of frequency combs [21], optical parametric oscillators [22], and entangled photon generation via four-wave mixing [23].

Remarkably, InGaP also possesses a large second-order susceptibility ( $\chi_{xyz}^{(2)} = 220$  pm/V) [24] and a bandgap of 1.92 eV corresponding to a cutoff wavelength of 645 nm. This marks InGaP as another thin-film material, besides  $\text{Al}_x\text{Ga}_{1-x}\text{As}$  ( $x \approx 0.3$ ), that has the highest second-order susceptibility as well as a cutoff wavelength less than the second harmonics of the telecommunication C band light. However, what makes InGaP unique for second-order nonlinear optics involving the telecommunication C band light is the fact that its antibonding anion state lies well above the bandgap [13], which avoids anion state-induced absorption below the bandgap. In contrast, the antibonding As-As surface state of  $\text{Al}_x\text{Ga}_{1-x}\text{As}$  lies below its bandgap [13], resulting in strong optical absorption at wavelengths shorter than 800 nm [11, 12]. In addition, the transparency window of InGaP extends to  $\sim 11$   $\mu\text{m}$  [25], which will enable applications in the mid-infrared wavelength band, including optical parametric oscillators [26, 27], detectors [28], and quantum cascade lasers [29].

## III. INGAP NONLINEAR PHOTONIC INTEGRATED CIRCUITS

Because InGaP has a similar refractive index as the GaAs substrate from which it is grown, in order to confine light in the InGaP thin-film photonic structures, it needs to be separated from the GaAs substrate. This can be achieved by transferring the InGaP thin film to a low-index substrate using various wafer bonding methods, including adhesive bonding [30] and, more recently, low-temperature plasma-activated bonding [31]. However, wafer bonding or flip-chip bonding can be challenging, requiring special tools and complicated processing. Instead, we developed a transfer-free method that makes suspended InGaP photonic integrated circuits in the InGaP-on-GaAs platform. The fabrication process is illustrated in Fig. 2a. Starting from the InGaP-on-GaAs epitaxial stack, the device pattern is defined using electron beam lithography and transferred to the InGaP thin film via inductively coupled plasma reactive-ion etch (ICP-RIE) using a mixture of  $\text{Cl}_2/\text{CH}_4/\text{Ar}$  gas. Then a thin layer of  $\text{Al}_2\text{O}_3$  is deposited on the sample via atomic layer deposition (ALD) followed by patterning the releasing holes in the  $\text{Al}_2\text{O}_3$  layer. Finally, the InGaP device is released from the GaAs substrate using selective wet etching. More details of the fabrication process are provided in Refs. [32, 33]. Figs. 2b and c show scanning electron microscope (SEM) images of the fabricated InGaP photonic integrated circuits, including waveguide-coupled microring resonators and meander waveguides.

### A. Microring resonators

In order to exploit the second-order susceptibility  $\chi_{xyz}^{(2)}$  of InGaP for second-order nonlinear optics, transverse-electric modes ( $\text{TE}_{00}$ ) and transverse-magnetic modes ( $\text{TM}_{00}$ ) of the microring resonator are used for the fundamental- and second-harmonics, respectively. The fundamental-harmonic (FH) and second-harmonic (SH)

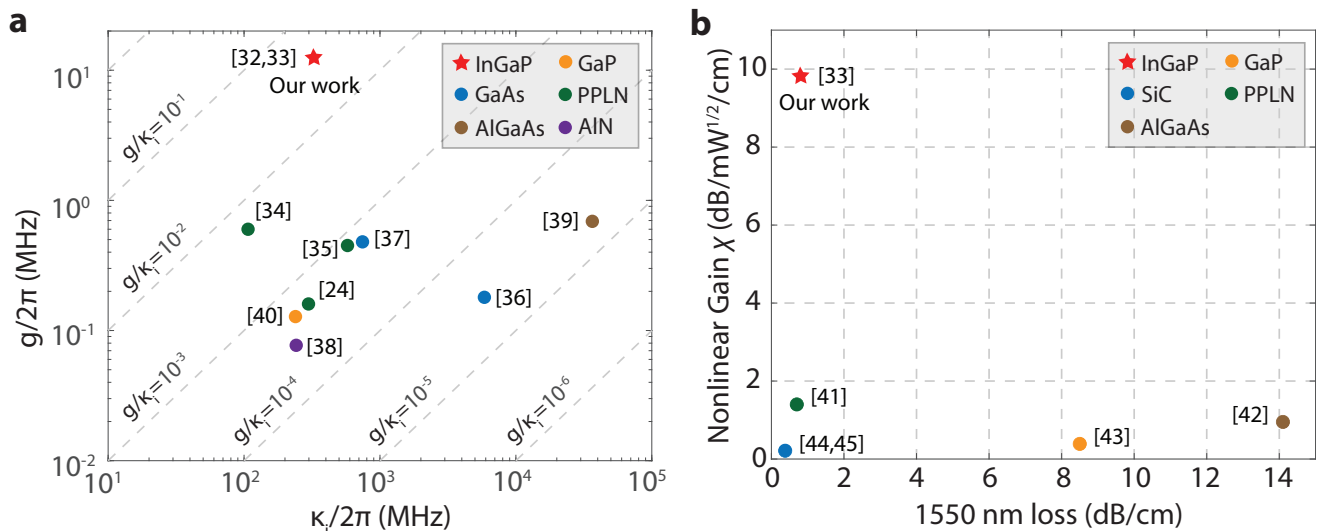


FIG. 3. **a**. Nonlinear mode coupling coefficient ( $g$ ) and intrinsic photon loss rate of the fundamental mode ( $\kappa_i$ ) of microring resonators made in second-order nonlinear photonics platforms, including InGaP: [32, 33], PPLN: [24, 34, 35], GaAs: [36, 37], AIN: [38], AlGaAs: [39], GaP: [40]. **b**. Nonlinear gain  $\chi$  and 1550 nm wavelength band loss of nanophotonic waveguides made in second-order nonlinear photonics platforms. InGaP: [33], PPLN: [41], AlGaAs: [42], GaP: [43], SiC: [44, 45].

modes,  $a$  and  $b$ , satisfy the frequency- and phase-matching conditions [32]:  $\omega_b = 2\omega_a$  and  $m_b = 2m_a \pm 2$ , where  $m_k$  is the azimuthal number of mode  $k$ . This can be achieved by designing the width of the microring for a given InGaP thickness. For phase matching between the telecommunication band FH mode and the corresponding SH mode, the thickness of InGaP should be around 110 nm [32].

The quality factor of the InGaP microring resonator depends on the ALD material used to suspend the microring resonator [33]. The intrinsic quality factor ( $Q_{ai}$ ) of 1550 nm band TE<sub>00</sub> resonances of the fabricated microring with 5  $\mu\text{m}$  radius and 1  $\mu\text{m}$  width is  $4 - 6 \times 10^5$  for ALD Al<sub>2</sub>O<sub>3</sub>, which is approximately  $2 - 3 \times$  higher than that of microring resonators with ALD SiO<sub>2</sub>. This is likely due to the passivation effect of Al<sub>2</sub>O<sub>3</sub> [46]. The intrinsic quality factor of 775 nm band TM<sub>00</sub> resonances of the same microring is  $1 - 2 \times 10^5$ , and is nearly independent of the ALD material.

The nonlinear interaction between the FH and SH modes can be described by the Hamiltonian,  $\hat{H} = g(\hat{a}^2\hat{b}^\dagger + \hat{a}^\dagger\hat{b}^2)$ , where  $\hat{a}$  ( $\hat{b}$ ) and  $\hat{a}^\dagger$  ( $\hat{b}^\dagger$ ) are the annihilation and creation operators for mode  $a$  ( $b$ ). The nonlinear coupling  $g$  is inferred from the second-harmonic generation (SHG) efficiency of the microring. For the phase-matched 5  $\mu\text{m}$ -radius microring, we find  $g/2\pi \approx 11$  MHz [32], which is consistent with the simulation. The nonlinear coupling scales with the microring radius approximately as  $g \propto \frac{1}{\sqrt{R}}$ .

A nonlinearity-to-loss ratio,  $g/\kappa_{ai}$ , where  $\kappa_{ai} \equiv \omega_a/Q_{ai}$ , can be defined to characterize the nonlinear cavity. Almost all second-order nonlinear optical effects of the cavity are determined by this ratio. Table I summa-

rizes the relation between the key metrics of several nonlinear optical processes and the nonlinearity-to-loss ratio. The 5  $\mu\text{m}$ -radius InGaP microring with  $Q_{ai} = 6 \times 10^5$  achieves a high  $g/\kappa_{ai} = 3.5\%$ . In Fig. 3a, we compare the nonlinearity-to-loss ratio of the state-of-the-art InGaP microring with microring resonators made in other  $\chi^{(2)}$  nonlinear photonics platforms.

TABLE I. Cavity  $\chi^{(2)}$  process

$\chi^{(2)}$ process	Metric	Scaling
SHG	Efficiency	$g^2/\kappa_{ai}^2\kappa_{bi}$ [47]
SPDC	Pair generation rate	$g^2/\kappa_{ai}\kappa_{bi}$ [48]
OPO	Pump threshold	$\kappa_{ai}^2\kappa_{bi}/g^2$ [49]
Squeezed light	Pump power	$\kappa_{ai}^2\kappa_{bi}/g^2$ [49]

SPDC: spontaneous parametric down-conversion. OPO: optical parametric oscillation. Pump power for squeezed light is assumed for optimal quadrature noise squeezing (i.e.,  $\kappa_{a,i}/\kappa_a$ ) on resonance. Critical coupling ( $\kappa_i = \kappa/2$ ) is assumed.

## B. Waveguides

Broadband second-order nonlinear optical effects can be realized in waveguides as opposed to microring resonators. Similar to the microring resonator, TE<sub>00</sub> and TM<sub>00</sub> modes of the waveguide are used for the fundamental- and second-harmonics, respectively. By designing the waveguide width for a given InGaP thickness, the two modes can satisfy the frequency- and phase-matching conditions:  $\omega_b = 2\omega_a$  and  $k_b = 2k_a$ , which lead

TABLE II. Waveguide  $\chi^{(2)}$  process

$\chi^{(2)}$ process	Metric	Relation
SPDC	Pair generation efficiency	$\frac{\hbar\omega_p L^{3/2}}{12\sqrt{2\pi} \text{GVD}(\frac{\omega_p}{2}) } \chi^2$ [50]
	Bandwidth	$\frac{\alpha}{\sqrt{ \text{GVD}(\frac{\omega_p}{2}) }L}$ [50]
OPA	Gain	$e^{\chi\sqrt{P_p}L}$ (maximum gain of PSA); $\frac{1}{4}e^{\chi\sqrt{P_p}L}$ (PIA)
	Bandwidth	$\frac{\alpha}{\sqrt{ \text{GVD}(\frac{\omega_p}{2}) }L}$
Squeezed light	Squeeze ratio	$\epsilon e^{-\chi\sqrt{P_p}L} + 1 - \epsilon$ [51]
Wavelength conversion	Conversion efficiency	$\sin^2(\chi\sqrt{P_p}L/\sqrt{2})$

GVD: group velocity dispersion.  $\alpha = \frac{1}{\pi}\sqrt{2\text{sinc}^{-1}\frac{1}{\sqrt{2}}}$ . OPA: optical parametric amplification. PSA: phase-sensitive amplifier. PIA: phase-insensitive amplifier.  $\epsilon = e^{-\gamma L}$ : aggregated waveguide loss. The waveguide loss is only considered for the squeezed light.

to  $n_b = n_a$ , where  $n_k$  is the effective mode index of mode  $k$ .

The phase-matched nonlinear waveguide can be characterized by its loss and nonlinear efficiency. The loss of the TE<sub>00</sub> mode of the InGaP waveguide in the 1550 nm band is measured to be  $\gamma = 0.8 \pm 0.4$  dB/cm [33], which is consistent with the intrinsic quality factor of the microring resonator (corresponding to 0.4 dB/cm). The difference might be due to the uncertainty of the fiber-optic coupling efficiency when measuring the waveguide transmission. The normalized SHG efficiency of the phase-matched InGaP waveguide is measured to be 128,000 %/W/cm<sup>2</sup> [33], which is consistent with the simulation value of 130,000 %/W/cm<sup>2</sup>. This is significantly higher than other demonstrations of InGaP  $\chi^{(2)}$  nonlinear waveguides [52, 53], which are limited by considerable optical losses and imperfect phase matching. The SHG efficiency of our InGaP nanophotonic waveguides is nearly two orders of magnitude higher than the thin-film periodically-poled LiNbO<sub>3</sub> (PPLN) waveguides in the telecommunication band [41, 54]. Such an enhancement in nonlinear efficiency can be understood via a back-of-the-envelope calculation. The normalized SHG efficiency of the InGaP waveguide can be calculated using [33]

$$\eta_{\text{SHG}} = \frac{\omega_a^2}{2n_a^2 n_b \epsilon_0 c^3} \left( \frac{\int d\mathbf{r} \chi_{xyz}^{(2)} \sum_{i \neq j \neq k} E_{bi}^* E_{aj} E_{ak}}{\int d\mathbf{r} |\mathbf{E}_a|^2 \sqrt{\int d\mathbf{r} |\mathbf{E}_b|^2}} \right)^2, \quad (1)$$

where the normalization integrals use electric field components perpendicular to the wavevector of the waveguide mode. Based on Eq. 1, the ratio between the nonlinear efficiency of InGaP and PPLN waveguides is estimated to be:  $(4 \times 2 \times \frac{\pi}{2})^2 \approx 160$ , where  $4 \times$  is from  $\chi_{xyz}^{(2)}$  of InGaP versus  $\chi_{zzz}^{(2)}$  of LiNbO<sub>3</sub>,  $2 \times$  is from the swap of indices  $x$  and  $y$  in  $\chi_{xyz}^{(2)}$  for InGaP, and  $1/\frac{2}{\pi} \times$  is due

to the periodic poling of LiNbO<sub>3</sub>. This estimation does not consider the difference in the mode overlap integral, which is generally an  $O(1)$  factor.

Using the normalized SHG efficiency, we can introduce a nonlinear gain defined as

$$\chi \equiv 2\sqrt{\eta_{\text{SHG}}}. \quad (2)$$

The nonlinear gain is convenient to characterize second-order nonlinear optical processes in the waveguide, including optical parametric amplification and squeezed light generation. Table II summarizes the key metrics of several second-order nonlinear optical processes of the waveguide as functions of the nonlinear gain  $\chi$  and waveguide loss. Fig. 3b compares the nonlinear gain and waveguide loss of the InGaP platform with other  $\chi^{(2)}$  nonlinear photonics platforms. In this plot, the numerical value of the nonlinear gain is calculated via  $\chi$  [dB/ $\sqrt{\text{mW}}/\text{cm}$ ] =  $10\log(e^{2\sqrt{\eta_{\text{SHG}}}})$ . The InGaP waveguide achieves  $\chi = 9.8$  dB/ $\sqrt{\text{mW}}/\text{cm}$ , which is significantly greater than other platforms.

#### IV. QUANTUM OPTICS: CAVITY

The nonlinearity-to-loss ratio of a few percent achieved in InGaP microring resonators enables quantum optical effects using passive bulk  $\chi^{(2)}$  nonlinearity at the few- and single-photon levels. Creating quantum correlations between initially uncorrelated photons, such as photon antibunching and photon blockade, are fundamental quantum optical effects and useful quantum resources. This is usually achieved using quantum emitters [55] or quantum interference induced by ancillary pumps [56]. Recently it was theoretically shown that photon antibunching and photon blockade can be achieved via passive bulk nonlinearities that are not necessarily in



the strong coupling regime [57]. Consider two uncorrelated photons propagate through a waveguide-coupled  $\chi^{(2)}$  nonlinear cavity. The wavefunction of the two photons after traversing the system consists of the nonlinear interaction-mediated amplitude  $T$  and the linear transmission amplitude  $t^2$ , where  $t$  is the single-photon transmission coefficient, leading to a normalized second-order correlation function [57]:

$$g^{(2)}(\tau) = \frac{|t_\omega^2 + T(\omega, \tau)|^2}{|t_\omega^2|^2}, \quad (3)$$

where  $\omega$  denotes the frequency of the photons and  $|T| \sim (g/\kappa)^2$ . As a result, quantum correlations between photons, such as photon antibunching and photon blockade, can be achieved by controlling the single-photon transmission coefficient of the photonic circuit such that  $t_\omega^2 + T(\omega, \tau) \approx 0$ , even for  $g/\kappa < 1$ . Initial experimental demonstration of such an effect has been realized using a waveguide-coupled InGaP microring resonator [58], where photon antibunching (i.e.,  $g^{(2)}(0) < g^{(2)}(\tau)$  for some  $\tau$ ) was observed. However, due to the free-standing InGaP device structure, thermal noises associated with the inherent mechanical vibrational modes of the device prevented the realization of photon blockade, i.e.,  $g^{(2)}(0) \approx 0$ . We expect this issue to be solved by adopting the InGaP-on-insulator device structure, which is free of vibrational modes.

The highly nonlinear InGaP cavity also enables nonlinear-optical entangling operations that facilitate quantum communications and quantum networking. Existing quantum networking protocols, such as quantum teleportation and entanglement swapping, rely on linear-optical Bell state measurements to herald the distribution and transfer of quantum information. However, the linear-optical Bell state measurement necessitates identical photons, making them prone to errors from multiphoton emissions [59, 60]. This dependency limits both the efficiency and fidelity of entanglement distribution. Additionally, any deviation in the input photons' identity can compromise the protocol's fidelity [61, 62]. A solution to this issue is the nonlinear-optical Bell state measurement, which uses the sum-frequency generation (SFG) process to filter out multiphoton emissions. This approach also mitigates the need for quantum interference of identical photons; instead, the input photons only need to meet the phase-matching condition for sum-frequency generation. Deviations from this condition primarily impact efficiency rather than fidelity. Recently, as reported in [63], we demonstrated the nonlinear Bell state measurement by exploiting an InGaP nonlinear cavity with a single-photon SFG probability ( $4 \times 10^{-5}$ ) over three orders of magnitude beyond prior nonlinear waveguides [64–67]. Using the nanophotonic nonlinear Bell state analyzer, we achieved faithful quantum teleportation involving time-bin encoded, spectrally-distinct photons with a fidelity  $\geq 94\%$  down to the single-photon level and validated the robustness of this scheme against multi-

photon emission. Beyond quantum teleportation, a nonlinear Bell state analyzer with even moderate SFG efficiency can facilitate faithful heralded entanglement swapping [68]—a crucial protocol for quantum repeaters—more efficiently than linear-optical protocols using ancillae [69, 70].

## V. QUANTUM OPTICS: WAVEGUIDE

In this section, we analyze several nonlinear and quantum optical processes in waveguides and highlight the advantage of the InGaP platform. One application of the  $\chi^{(2)}$  nonlinear waveguide is for entangled photon pair generation via SPDC. The relations of the pair generation efficiency ( $P_{\text{SPDC}}/P_p$ ) and the bandwidth of the SPDC photons of a phase-matched waveguide are given in Table II. Recently, we demonstrated an ultra-bright, broadband, time-energy entangled photon source utilizing the InGaP nanophotonic waveguide [33]. A 1.6 mm long InGaP waveguide achieves a pair generation rate of 97 GHz/mW and a bandwidth of 14.4 THz (115 nm) centered at the telecommunication C band. This corresponds to a per-bandwidth pair generation efficiency of 6.7 GHz/mW/THz (840 MHz/mW/nm). The ultrahigh rate efficiency of the InGaP nanophotonic waveguide can be understood from the fact that the pair generation efficiency is proportional to the SHG efficiency (Table II). In Fig. 4, we compare the InGaP nanophotonic waveguide SPDC source with other broadband SPDC sources, including bulk crystals and waveguides. The InGaP waveguide SPDC source exhibits a leading pair generation efficiency with a large bandwidth, underscoring its potential for quantum information applications.

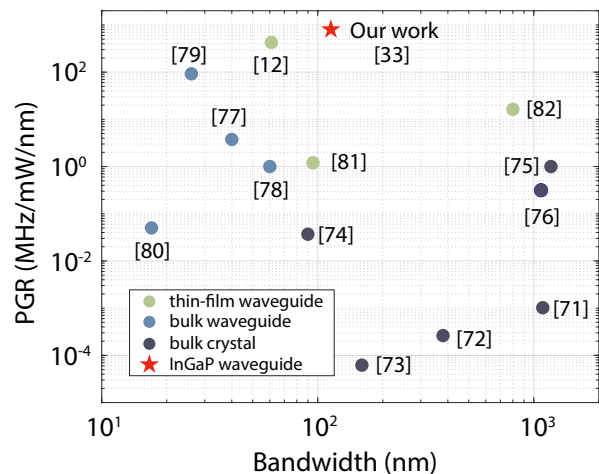


FIG. 4. Per-bandwidth pair generation rate (PGR) and bandwidth of recently demonstrated broadband SPDC sources. Bulk crystal: [71–76]. Bulk waveguide: [77–80]. Thin-film waveguide: [12, 33, 81, 82].

Another application of  $\chi^{(2)}$  nonlinear waveguides is for

traveling-wave optical parametric amplifiers (OPAs). In this case, a pump light of frequency  $\omega_p$  and a signal light of frequency  $\omega_s$ , satisfying  $\omega_p \approx 2\omega_s$ , are injected into the  $\chi^{(2)}$  nonlinear waveguide. When the waveguide satisfies the phase-matching condition, the three-wave mixing process transfers energy from the pump to amplify the signal. For a waveguide that is phase-matched for the degenerate three-wave mixing process, the bandwidth of the traveling-wave OPA is identical to that of the SPDC photons (Table II), determined by the waveguide length and the group velocity dispersion of the waveguide. When the frequencies of the pump and signal satisfy  $\omega_p = 2\omega_s$ , the OPA is phase-sensitive, i.e., the gain depends on the phase of the signal. In this case, the maximum gain is given by

$$G_{\text{PSA}} = e^{\chi\sqrt{P_p}L}, \quad (4)$$

where  $\chi$  is the nonlinear gain introduced in Eq. 2,  $P_p$  is the pump power, and  $L$  is the length of the waveguide. When the frequencies of the pump and signal do not satisfy the double relationship and the signal lies in the phase-matching bandwidth, the OPA is phase-insensitive and the constant gain is given by

$$G_{\text{PIA}} = \cosh^2(\chi\sqrt{P_p}L/2) \approx \frac{1}{4}e^{\chi\sqrt{P_p}L}. \quad (5)$$

Essentially, the gain of a phase-insensitive OPA is 6 dB less than the maximum gain of a phase-sensitive OPA [83]. From the measured nonlinear gain  $\chi = 9.8$  dB/ $\sqrt{\text{mW}}/\text{cm}$  of the InGaP waveguide, we expect a maximum gain of 30 dB can be achieved in a 1 cm long InGaP waveguide with only 10 mW on-chip pump power. The InGaP OPA empowered by its extreme  $\chi^{(2)}$  nonlinearity is expected to transcend the state-of-the-art integrated traveling-wave OPAs based on Kerr nonlinearity [84, 85], in terms of pump efficiency, device size, and noise figure.

Related to the OPA,  $\chi^{(2)}$  nonlinear waveguides can be used for generating squeezed light. When the waveguide is pumped at frequency  $\omega_p$ , squeezed vacuum at the frequency of  $\omega_p/2$  or two-mode squeezed light at frequencies  $\omega_p/2 \pm \Delta$  can be generated. The quantum fluctuation of one quadrature of the squeezed vacuum (or the sum of one quadrature of the two-mode squeezed light) is de-amplified while that of the orthogonal quadrature (or the sum of the orthogonal quadrature) is amplified. Waveguide loss needs to be considered for the squeezed light since it corresponds to the vacuum noise. The squeeze ratio  $R$ , defined as the reduction of the quadrature noise power, of the squeezed vacuum and the two-mode squeezed light generated in a phase-matched  $\chi^{(2)}$  nonlinear waveguide is given by [51]

$$R = \epsilon e^{-\chi\sqrt{P_p}L} + 1 - \epsilon, \quad (6)$$

where  $\epsilon = e^{-\gamma L}$  is the aggregated waveguide loss. According to Eq. 6, for a given pump power, there ex-

ists an optimal waveguide length to achieve the maximum squeeze ratio, due to the trade-off between the parametric gain and waveguide loss. For example, using the measured nonlinear gain  $\chi = 9.8$  dB/ $\sqrt{\text{mW}}/\text{cm}$  and waveguide loss of 0.8 dB/cm, for  $P_p = 10(100)$  mW, an optimal squeezing of 9.5(13.5) dB can be achieved with a 5(2) mm long InGaP waveguide. This predicted squeezing level is significantly higher than current integrated squeezed light demonstrations using continuous-wave pumps, where the reported squeezing is around 2 dB [86–89] with one experiment reaching 6 dB [90], and is comparable to the record of squeezing (15 dB) achieved using bulk nonlinear crystals [91].

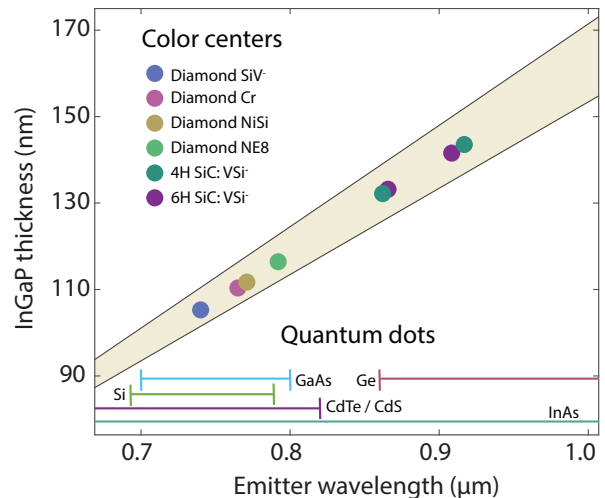


FIG. 5. Quantum wavelength conversion to 1550 nm through DFG for solid-state quantum emitters. Shaded area indicates the thickness of InGaP that realizes the phase-matching condition. The emission range of quantum dots are represented using line segments at the bottom. Defect color centers, diamond SiV: [92], diamond Cr: [92], diamond NiSi: [93, 94], diamond NE8: [95],  $\text{V}_{\text{Si}}^-$  in 4H SiC [96, 97] and 6H SiC: [96]. Quantum dots, InAs: [98], GaAs: [99, 100], CdTe/CdS [101], Si: [102], Ge: [103].

Finally, we consider quantum wavelength conversion using the InGaP nonlinear waveguide. To unify quantum platforms operating at different wavelengths and establish quantum networks utilizing optical fibers, quantum wavelength conversion of photons emitted by matter qubits to telecommunication C band photons is desirable. InGaP has a cutoff wavelength of 650 nm and low optical absorption below the bandgap, which makes it suitable for quantum wavelength conversion involving a variety of quantum emitters. We consider quantum wavelength conversion from quantum emitter wavelengths in the 670 – 1010 nm range to 1550 nm via different-frequency generation (DFG) with a pump wavelength longer than the emitter wavelength. We design InGaP-on-insulator ( $\text{SiO}_2$ ) waveguides satisfying the phase-matching condition for such DFG processes. To this end, we limit the waveguide width to be in the range between 1  $\mu\text{m}$  and

5  $\mu\text{m}$ , and identify the proper thickness of the InGaP such that the phase-matching condition can be realized for a given emitter wavelength. The shaded region in Fig. 5 shows the range of desired InGaP thickness depending on the emitter wavelength. Several solid-state defect centers and quantum dots emit in the wavelength range of 670 – 1010 nm considered here. For example, the  $\text{SiV}^-$  center in diamond has a zero phonon line (ZPL) at 740 nm [104] and the two types of  $\text{V}_{\text{Si}}^-$  center in 4H-SiC have ZPL at 862 nm and 917 nm [96, 97]. On the other hand, quantum dots can emit into a wide wavelength band depending on their composition and sizes, e.g., InAs (700 – 1200 nm) [98], GaAs (700 – 800 nm) [99, 100], Si (693 – 789 nm) [102], CdTe/CdS (480 – 820 nm) [101] and Ge (860 – 1230 nm) [103]. The quantum efficiency of wavelength conversion from the photon of wavelength  $\lambda_1$  to the photon of target wavelength  $\lambda_2$  is given by

$$F_{\lambda_2}(L)/F_{\lambda_1}(0) = \sin^2(\chi\sqrt{P_p}L/\sqrt{2}), \quad (7)$$

where  $F_{\lambda}(x)$  is the photon number flux at position  $x$  and we have ignored waveguide loss. Thus the waveguide length to achieve unit-efficiency conversion is

$$L_{\pi} = \pi/(\chi\sqrt{2P_p}). \quad (8)$$

Assuming the nonlinear gain of the waveguide for DFG is similar to that of the waveguide for SHG, we estimate  $L_{\pi} = 3.1(9.8)$  mm for pump power  $P_p = 10(1)$  mW. Such pump powers for high-efficiency quantum wavelength conversion are significantly lower than the state of the art and will reduce parasitic noises that hamper quantum wavelength conversion.

## VI. CONCLUSION

In this Perspective, we provided a brief review of the newly developed epitaxial InGaP integrated  $\chi^{(2)}$  nonlinear photonics platform and discussed its applications in quantum and nonlinear optics. Leveraging its exceptional nonlinearity and low optical loss, the InGaP platform has achieved highly efficient  $\chi^{(2)}$  nonlinear optical effects, surpassing the current state of the art, such as second-harmonic generation and entangled photon pair generation via SPDC. Addi-

tionally, the InGaP platform enables novel quantum optical effects at the few- and single-photon levels, which are crucial for quantum information processing and quantum networking. However, addressing certain challenges is necessary to fully realize the potential of the InGaP platform. The first challenge is to realize the InGaP-on-insulator platform, which will help mitigate parasitic noises for quantum optics and facilitate high optical powers for applications involving waveguide devices. Recently, the InGaP-on-insulator structure via low-temperature plasma-activated wafer bonding has been reported [31]. However, the reported optical loss is still worse than the suspended InGaP platform. Further optimization of the wafer bonding process to reduce optical losses is necessary. Another challenge is the thickness nonuniformity of the epitaxial InGaP thin film. The phase-matching condition for second-order nonlinear optical processes is highly sensitive to the InGaP thickness. This is in general not relevant for microcavities, as the thickness variation occurs at a much larger scale, but will impact waveguides with a considerable length, leading to reduced nonlinear efficiency. Growth condition optimization and the adapted waveguide approach [105] might be able to overcome this challenge. With these current obstacles addressed, the InGaP  $\chi^{(2)}$  nonlinear photonics platform is expected to yield unparalleled performances for a broad range of classical and quantum applications, including optical parametric amplification, squeezed light generation, and quantum wavelength conversion, to name a few.

### Data availability

All data used in this study are available from the corresponding authors upon reasonable request.

### Acknowledgements

This work was supported by US National Science Foundation (Grant No. ECCS-2223192), NSF Quantum Leap Challenge Institute QLCI-HQAN (Grant No. 2016136), and U.S. Department of Energy Office of Science National Quantum Information Science Research Centers.

### Conflict of interest

The authors declare no competing interests.

- 
- [1] Joseph Anthony Giordmaine and Robert C Miller, “Tunable coherent parametric oscillation in  $\text{LiNbO}_3$  at optical frequencies,” *Physical Review Letters* **14**, 973 (1965).
- [2] Shambhu Ghimire, Anthony D DiChiara, Emily Sistrunk, Pierre Agostini, Louis F DiMauro, and David A Reis, “Observation of high-order harmonic generation in a bulk crystal,” *Nature Physics* **7**, 138–141

- (2011).
- [3] Yong Sing You, David A Reis, and Shambhu Ghimire, “Anisotropic high-harmonic generation in bulk crystals,” *Nature Physics* **13**, 345–349 (2017).
- [4] Paul G Kwiat, Klaus Mattle, Harald Weinfurter, Anton Zeilinger, Alexander V Sergienko, and Yanhua Shih, “New high-intensity source of polarization-entangled photon pairs,” *Physical Review Letters* **75**, 4337 (1995).

- [5] Roman Schnabel, “Squeezed states of light and their applications in laser interferometers,” *Physics Reports* **684**, 1–51 (2017).
- [6] Nicolas Gisin and Rob Thew, “Quantum communication,” *Nature Photonics* **1**, 165–171 (2007).
- [7] Benjamin J Lawrie, Paul D Lett, Alberto M Marino, and Raphael C Pooser, “Quantum sensing with squeezed light,” *Acs Photonics* **6**, 1307–1318 (2019).
- [8] Jeremy L O’Brien, “Optical quantum computing,” *Science* **318**, 1567–1570 (2007).
- [9] Avik Dutt, Aseema Mohanty, Alexander L Gaeta, and Michal Lipson, “Nonlinear and quantum photonics using integrated optical materials,” *Nature Reviews Materials* **9**, 321–346 (2024).
- [10] M. Ohashi, T. Kondo, R. Ito, S. Fukatsu, Y. Shiraki, K. Kumata, and S.S. Kano, “Determination of quadratic nonlinear optical coefficient of  $\text{Al}_x\text{Ga}_{1-x}\text{As}$  system by the method of reflected second harmonics,” *Journal of Applied Physics* **74**, 596–601 (1993).
- [11] C.P. Michael, K. Srinivasan, T.J. Johnson, O. Painter, K.H. Lee, K. Hennessy, H. Kim, and E. Hu, “Wavelength- and material-dependent absorption in GaAs and AlGaAs microcavities,” *Applied Physics Letters* **90**, 051108 (2007).
- [12] Marlon Placke, Jan Schlegel, Felix Mann, Pietro Della Casa, Andreas Thies, Markus Weyers, Günther Tränkle, and Sven Ramelow, “Telecom-Band Spontaneous Parametric Down-Conversion in AlGaAs-on-Insulator Waveguides,” *Laser & Photonics Reviews* **18**, 2301293 (2024).
- [13] Liang Lin and John Robertson, “Passivation of interfacial defects at III-V oxide interfaces,” *Journal of Vacuum Science & Technology B* **30** (2012).
- [14] Tatsuya Takamoto, Minoru Kaneiwa, Mitsuru Imaizumi, and Masafumi Yamaguchi, “InGaP/GaAs-based multijunction solar cells,” *Progress in Photovoltaics: Research and Applications* **13**, 495–511 (2005).
- [15] C. Patrik T. Svensson, Thomas Mårtensson, Johanna Trägårdh, Christina Larsson, Michael Rask, Dan Hesselman, Lars Samuelson, and Jonas Ohlsson, “Monolithic GaAs/InGaP nanowire light emitting diodes on silicon,” *Nanotechnology* **19**, 305201 (2008).
- [16] J. Jiang, S. Tsao, T. O’Sullivan, W. Zhang, H. Lim, T. Sills, K. Mi, M. Razeghi, G.J. Brown, and M.Z. Tidrow, “High detectivity InGaAs/InGaP quantum-dot infrared photodetectors grown by low pressure metalorganic chemical vapor deposition,” *Applied Physics Letters* **84**, 2166–2168 (2004).
- [17] N. Pan, J. Elliott, M. Knowles, D.P. Vu, K. Kishimoto, J.K. Twynam, H. Sato, M.T. Fresina, and G.E. Stillman, “High reliability InGaP/GaAs HBT,” *IEEE Electron Device Letters* **19**, 115–117 (1998).
- [18] HQ Zheng, SF Yoon, BP Gay, KW Mah, K Radhakrishnan, and GI Ng, “Growth optimization of InGaP layers by solid source molecular beam epitaxy for the application of InGaP/In<sub>0.2</sub>Ga<sub>0.8</sub>As/GaAs high electron mobility transistor structures,” *Journal of Crystal Growth* **216**, 51–56 (2000).
- [19] V. Eckhouse, I. Cestier, G. Eisenstein, S. Combrié, P. Colman, A. De Rossi, M. Santagiustina, C.G. Someda, and G. Vadalà, “Highly efficient four wave mixing in GaInP photonic crystal waveguides,” *Optics Letters* **35**, 1440–1442 (2010).
- [20] Pierre Colman, Chad Husko, Sylvain Combrié, Isabelle Sagnes, Chee Wei Wong, and Alfredo De Rossi, “Temporal solitons and pulse compression in photonic crystal waveguides,” *Nature Photonics* **4**, 862–868 (2010).
- [21] Utsav D. Dave, Charles Ciret, Simon-Pierre Gorza, Sylvain Combrie, Alfredo De Rossi, Fabrice Raineri, Gunther Roelkens, and Bart Kuyken, “Dispersive-wave-based octave-spanning supercontinuum generation in InGaP membrane waveguides on a silicon substrate,” *Optics Letters* **40**, 3584–3587 (2015).
- [22] Gabriel Marty, Sylvain Combrié, Fabrice Raineri, and Alfredo De Rossi, “Photonic crystal optical parametric oscillator,” *Nature Photonics* **15**, 53–58 (2021).
- [23] Alexandre Chopin, Andrea Barone, Inès Ghorbel, Sylvain Combrié, Daniele Bajoni, Fabrice Raineri, Matteo Galli, and Alfredo De Rossi, “Ultra-efficient generation of time-energy entangled photon pairs in an InGaP photonic crystal cavity,” *Communications Physics* **6**, 77 (2023).
- [24] Yoshiyasu Ueno, Vincent Ricci, and George I. Stegeman, “Second-order susceptibility of  $\text{Ga}_{0.5}\text{In}_{0.5}\text{P}$  crystals at  $1.5\ \mu\text{m}$  and their feasibility for waveguide quasi-phase matching,” *JOSA B* **14**, 1428–1436 (1997).
- [25] Dalziel J Wilson, Katharina Schneider, Simon Hönl, Miles Anderson, Yannick Baumgartner, Lukas Czornomaz, Tobias J Kippenberg, and Paul Seidler, “Integrated gallium phosphide nonlinear photonics,” *Nature Photonics* **14**, 57–62 (2020).
- [26] Alireza Marandi, Nick C Leindecker, Vladimir Pervak, Robert L Byer, and Konstantin L Vodopyanov, “Coherence properties of a broadband femtosecond mid-ir optical parametric oscillator operating at degeneracy,” *Optics express* **20**, 7255–7262 (2012).
- [27] Markku Vainio and Lauri Halonen, “Mid-infrared optical parametric oscillators and frequency combs for molecular spectroscopy,” *Physical Chemistry Chemical Physics* **18**, 4266–4294 (2016).
- [28] Manijeh Razeghi and Binh-Minh Nguyen, “Advances in mid-infrared detection and imaging: a key issues review,” *Reports on Progress in Physics* **77**, 082401 (2014).
- [29] Yu Yao, Anthony J Hoffman, and Claire F Gmachl, “Mid-infrared quantum cascade lasers,” *Nature Photonics* **6**, 432–439 (2012).
- [30] Utsav D. Dave, Bart Kuyken, François Leo, Simon-Pierre Gorza, Sylvain Combrie, Alfredo De Rossi, Fabrice Raineri, and Gunther Roelkens, “Nonlinear properties of dispersion engineered InGaP photonic wire waveguides in the telecommunication wavelength range,” *Optics Express* **23**, 4650–4657 (2015).
- [31] Lillian Thiel, Joshua E Castro, Trevor J Steiner, Catherine L Nguyen, Audrey Pechilis, Liao Duan, Nicholas Lewis, Garrett D Cole, John E Bowers, and Galan Moody, “Wafer-scale fabrication of ingap-on-insulator for nonlinear and quantum photonic applications,” arXiv preprint arXiv:2406.18788 (2024).
- [32] Mengdi Zhao and Kejie Fang, “InGaP quantum nanophotonic integrated circuits with 1.5% nonlinearity-to-loss ratio,” *Optica* **9**, 258–263 (2022).
- [33] Joshua Akin, Yunlei Zhao, Yuvraj Misra, AKM Naziul Haque, and Kejie Fang, “InGaP  $\chi^{(2)}$  integrated photonics platform for broadband, ultra-efficient nonlinear conversion and entangled photon generation,” *Light: Science & Applications* **11**, 1–10 (2022).

- ence & Applications **13**, 290 (2024).
- [34] Juanjuan Lu, Ming Li, Chang-Ling Zou, Ayed Al Sayem, and Hong X. Tang, “Toward 1% single-photon anharmonicity with periodically poled lithium niobate microring resonators,” *Optica* **7**, 1654–1659 (2020).
- [35] Zhaohui Ma, Jia-Yang Chen, Zhan Li, Chao Tang, Yong Meng Sua, Heng Fan, and Yu-Ping Huang, “Ultrabright quantum photon sources on chip,” *Physical Review Letters* **125**, 263602 (2020).
- [36] Paulina S Kuo, Jorge Bravo-Abad, and Glenn S Solomon, “Second-harmonic generation using-quasi-phasematching in a GaAs whispering-gallery-mode microcavity,” *Nature Communications* **5**, 3109 (2014).
- [37] Lin Chang, Andreas Boes, Paolo Pintus, Jon D Peters, MJ Kennedy, Xiao-Wen Guo, Nicolas Volet, Su-Peng Yu, Scott B Papp, and John E Bowers, “Strong frequency conversion in heterogeneously integrated GaAs resonators,” *APL Photonics* **4**, 036103 (2019).
- [38] Alexander W Bruch, Xianwen Liu, Xiang Guo, Joshua B Surya, Zheng Gong, Liang Zhang, Junxi Wang, Jianchang Yan, and Hong X Tang, “17 000%/W second-harmonic conversion efficiency in single-crystalline aluminum nitride microresonators,” *Applied Physics Letters* **113**, 131102 (2018).
- [39] S Mariani, A Andronico, A Lemaître, I Favero, S Ducci, and G Leo, “Second-harmonic generation in AlGaAs microdisks in the telecom range,” *Optics Letters* **39**, 3062–3065 (2014).
- [40] Alan D Logan, Michael Gould, Emma R Schmidgall, Karine Hestroffer, Zin Lin, Weiliang Jin, Arka Majumdar, Fariba Hatami, Alejandro W Rodriguez, and Kai-Mei C Fu, “400%/W second harmonic conversion efficiency in 14  $\mu\text{m}$ -diameter gallium phosphide-on-oxide resonators,” *Optics Express* **26**, 33687–33699 (2018).
- [41] Cheng Wang, Carsten Langrock, Alireza Marandi, Marc Jankowski, Mian Zhang, Boris Desiatov, Martin M Fejer, and Marko Lončar, “Ultrahigh-efficiency wavelength conversion in nanophotonic periodically poled lithium niobate waveguides,” *Optica* **5**, 1438–1441 (2018).
- [42] Stuart May, Michael Kues, Matteo Clerici, and Marc Sorel, “Second-harmonic generation in AlGaAs-on-insulator waveguides,” *Optics Letters* **44**, 1339–1342 (2019).
- [43] Konstantinos Pantzas, Sylvain Combrié, Myriam Bailly, Raphaël Mandouze, Francesco Rinaldo Talenti, Abdelmounaim Harouri, Bruno Gérard, Grégoire Beaudoin, Luc Le Gratiet, Gilles Patriarche, *et al.*, “Continuous-wave second-harmonic generation in orientation-patterned gallium phosphide waveguides at telecom wavelengths,” *ACS Photonics* **9**, 2032–2039 (2022).
- [44] Yi Zheng, Ailun Yi, Chaochao Ye, Kresten Yvind, Han Zhang, Xin Ou, and Minhao Pu, “Efficient second-harmonic generation in silicon carbide nanowaveguides,” in *2022 Conference on Lasers and Electro-Optics (CLEO) (IEEE, 2022)* pp. 1–2.
- [45] Ailun Yi, Chengli Wang, Liping Zhou, Yifan Zhu, Shibin Zhang, Tianguai You, Jiaxiang Zhang, and Xin Ou, “Silicon carbide for integrated photonics,” *Applied Physics Reviews* **9**, 031302 (2022).
- [46] Biswarup Guha, Felix Marsault, Fabian Cadiz, Laurence Morgenroth, Vladimir Ulin, Vladimir Berkovitz, Aristide Lemaître, Carmen Gomez, Alberto Amo, Sylvain Combrié, *et al.*, “Surface-enhanced gallium arsenide photonic resonator with quality factor of  $6 \times 10^6$ ,” *Optica* **4**, 218–221 (2017).
- [47] Xiang Guo, Chang-Ling Zou, and Hong X Tang, “Second-harmonic generation in aluminum nitride microrings with 2500%/w conversion efficiency,” *Optica* **3**, 1126–1131 (2016).
- [48] Xiang Guo, Chang-ling Zou, Carsten Schuck, Hojoong Jung, Risheng Cheng, and Hong X Tang, “Parametric down-conversion photon-pair source on a nanophotonic chip,” *Light: Science & Applications* **6**, e16249–e16249 (2017).
- [49] Daniel F Walls and Gerard J Milburn, *Quantum Optics* (Springer Science & Business Media, 2007).
- [50] Ramesh Kumar and Joyee Ghosh, “Parametric down-conversion in pplN ridge waveguide: a quantum analysis for efficient twin photons generation at 1550 nm,” *Journal of Optics* **20**, 075202 (2018).
- [51] Hubert S Stokowski, Timothy P McKenna, Taewon Park, Alexander Y Hwang, Devin J Dean, Oguz Tolga Celik, Vahid Ansari, Martin M Fejer, and Amir H Safavi-Naeini, “Integrated quantum optical phase sensor in thin film lithium niobate,” *Nature Communications* **14**, 3355 (2023).
- [52] Nicolas Poulvellarie, Carlos Mas Arabi, Charles Ciret, Sylvain Combrié, Alfredo De Rossi, Marc Haelterman, Fabrice Raineri, Bart Kuyken, Simon-Pierre Gorza, and François Leo, “Efficient type II second harmonic generation in an indium gallium phosphide on insulator wire waveguide aligned with a crystallographic axis,” *Optics Letters* **46**, 1490–1493 (2021).
- [53] Albert Peralta Amores and Marcin Swillo, “Low Temperature Bonding of Nanolayered InGaP/SiO<sub>2</sub> Waveguides for Spontaneous-Parametric Down Conversion,” *ACS Applied Nano Materials* **5**, 2550–2557 (2022).
- [54] Pao-Kang Chen, Ian Briggs, Chaohan Cui, Liang Zhang, Manav Shah, and Linran Fan, “Adapted poling to break the nonlinear efficiency limit in nanophotonic lithium niobate waveguides,” *Nature Nanotechnology* **19**, 44–50 (2024).
- [55] Kevin M Birnbaum, Andreea Boca, Russell Miller, Allen D Boozer, Tracy E Northup, and H Jeff Kimble, “Photon blockade in an optical cavity with one trapped atom,” *Nature* **436**, 87–90 (2005).
- [56] H Flayac and V Savona, “Unconventional photon blockade,” *Physical Review A* **96**, 053810 (2017).
- [57] Yunkai Wang and Kejie Fang, “Few-photon transport via a multimode nonlinear cavity: theory and applications,” *Physical Review A* **105**, 023713 (2022).
- [58] Mengdi Zhao, Yunkai Wang, Shanhui Fan, and Kejie Fang, “Quantum correlated photons via a passive nonlinear microcavity,” *arXiv preprint arXiv:2304.11676* (2023).
- [59] Pieter Kok and Samuel L Braunstein, “Postselected versus nonpostselected quantum teleportation using parametric down-conversion,” *Physical Review A* **61**, 042304 (2000).
- [60] Jian-Wei Pan, Sara Gasparoni, Markus Aspelmeyer, Thomas Jennewein, and Anton Zeilinger, “Experimental realization of freely propagating teleported qubits,” *Nature* **421**, 721–725 (2003).
- [61] Nicolas Sangouard, Christoph Simon, Hugues De Riedmatten, and Nicolas Gisin, “Quantum repeaters based



- on atomic ensembles and linear optics,” *Reviews of Modern Physics* **83**, 33–80 (2011).
- [62] Koji Azuma, Sophia E Economou, David Elkouss, Paul Hilaire, Liang Jiang, Hoi-Kwong Lo, and Ilan Tzitrin, “Quantum repeaters: From quantum networks to the quantum internet,” *Reviews of Modern Physics* **95**, 045006 (2023).
- [63] Joshua Akin, Yunlei Zhao, Paul G Kwiat, Elizabeth A Goldschmidt, and Kejie Fang, “Faithful quantum teleportation via a nanophotonic nonlinear Bell state analyzer,” submitted.
- [64] Sebastien Tanzilli, Wolfgang Tittel, Mattheus Halder, Olivier Alibart, Pascal Baldi, Nicolas Gisin, and Hugo Zbinden, “A photonic quantum information interface,” *Nature* **437**, 116–120 (2005).
- [65] Thiago Guerreiro, Enrico Pomarico, Bruno Sanguinetti, Nicolas Sangouard, JS Pelc, C Langrock, MM Fejer, Hugo Zbinden, Robert T Thew, and Nicolas Gisin, “Interaction of independent single photons based on integrated nonlinear optics,” *Nature Communications* **4**, 2324 (2013).
- [66] Thiago Guerreiro, A Martin, B Sanguinetti, JS Pelc, C Langrock, MM Fejer, N Gisin, H Zbinden, N Sangouard, and RT Thew, “Nonlinear interaction between single photons,” *Physical Review Letters* **113**, 173601 (2014).
- [67] Paul Fisher, Robert Cernansky, Ben Haylock, and Mirko Lobino, “Single photon frequency conversion for frequency multiplexed quantum networks in the telecom band,” *Physical Review Letters* **127**, 023602 (2021).
- [68] Nicolas Sangouard, Bruno Sanguinetti, Noé Curtz, Nicolas Gisin, Rob Thew, and Hugo Zbinden, “Faithful entanglement swapping based on sum-frequency generation,” *Physical Review Letters* **106**, 120403 (2011).
- [69] Claudia Wagenknecht, Che-Ming Li, Andreas Reingruber, Xiao-Hui Bao, Alexander Goebel, Yu-Ao Chen, Qiang Zhang, Kai Chen, and Jian-Wei Pan, “Experimental demonstration of a heralded entanglement source,” *Nature Photonics* **4**, 549–552 (2010).
- [70] Stefanie Barz, Gunther Cronenberg, Anton Zeilinger, and Philip Walther, “Heralded generation of entangled photon pairs,” *Nature Photonics* **4**, 553–556 (2010).
- [71] Akira Tanaka, Ryo Okamoto, Hwan Hong Lim, Shanthi Subashchandran, Masayuki Okano, Labao Zhang, Lin Kang, Jian Chen, Peiheng Wu, Toru Hirohata, *et al.*, “Noncollinear parametric fluorescence by chirped quasi-phase matching for monocycle temporal entanglement,” *Optics Express* **20**, 25228–25238 (2012).
- [72] Masayuki Okano, Hwan Hong Lim, Ryo Okamoto, Norihiko Nishizawa, Sunao Kurimura, and Shigeki Takeuchi, “0.54  $\mu\text{m}$  resolution two-photon interference with dispersion cancellation for quantum optical coherence tomography,” *Scientific Reports* **5**, 18042 (2015).
- [73] Masayuki Okano, Ryo Okamoto, Akira Tanaka, Shanthi Subashchandran, and Shigeki Takeuchi, “Generation of broadband spontaneous parametric fluorescence using multiple bulk nonlinear crystals,” *Optics Express* **20**, 13977–13987 (2012).
- [74] Maria V Chekhova, Semen Germanskiy, Dmitri B Horoshko, Galiya Kh Kitaeva, Mikhail I Kolobov, Gerd Leuchs, Chris R Phillips, and Pavel A Prudkovskii, “Broadband bright twin beams and their upconversion,” *Optics Letters* **43**, 375–378 (2018).
- [75] Yaakov Shaked, Roey Pomerantz, Rafi Z Vered, and Avi Peer, “Observing the nonclassical nature of ultra-broadband bi-photons at ultrafast speed,” *New Journal of Physics* **16**, 053012 (2014).
- [76] Kevin A O’Donnell and Alfred B U’Ren, “Observation of ultrabroadband, beamlike parametric downconversion,” *Optics Letters* **32**, 817–819 (2007).
- [77] S Tanzilli, Wolfgang Tittel, Hugues De Riedmatten, Hugo Zbinden, Paolo Baldi, M DeMicheli, Da B Ostrowsky, and Nicolas Gisin, “PPLN waveguide for quantum communication,” *The European Physical Journal D-Atomic, Molecular, Optical and Plasma Physics* **18**, 155–160 (2002).
- [78] Yiwen Huang, Juan Feng, Yuanhua Li, Zhantong Qi, Chuangyi Lu, Yuanlin Zheng, and Xianfeng Chen, “High-performance hyperentanglement generation and manipulation based on lithium niobate waveguides,” *Physical Review Applied* **17**, 054002 (2022).
- [79] Bo Cao, Kyohei Hayama, Shun Suezawa, Mamoru Hisamitsu, Katsuhiko Tokuda, Sunao Kurimura, Ryo Okamoto, and Shigeki Takeuchi, “Non-collinear generation of ultra-broadband parametric fluorescence photon pairs using chirped quasi-phase matching slab waveguides,” *Optics Express* **31**, 23551–23562 (2023).
- [80] Alfred B U’Ren, Christine Silberhorn, Konrad Banaszek, and Ian A Walmsley, “Efficient Conditional Preparation of High-Fidelity Single Photon States for Fiber-Optic Quantum Networks,” *Physical Review Letters* **93**, 093601 (2004).
- [81] Dongpeng Kang, Ankita Anirban, and Amr S Helmy, “Monolithic semiconductor chips as a source for broadband wavelength-multiplexed polarization entangled photons,” *Optics Express* **24**, 15160–15170 (2016).
- [82] Usman A. Javid, Jingwei Ling, Jeremy Staffa, Mingxiao Li, Yang He, and Qiang Lin, “Ultrabroadband entangled photons on a nanophotonic chip,” *Physical Review Letters* **127**, 183601 (2021).
- [83] Peter A Andrekson and Magnus Karlsson, “Fiber-based phase-sensitive optical amplifiers and their applications,” *Advances in Optics and Photonics* **12**, 367–428 (2020).
- [84] Johann Riemensberger, Nikolai Kuznetsov, Junqiu Liu, Jijun He, Rui Ning Wang, and Tobias J. Kippenberger, “A photonic integrated continuous-travelling-wave parametric amplifier,” *Nature* **612**, 56–61 (2022).
- [85] Nikolai Kuznetsov, Alberto Nardi, Alisa Davydova, Mikhail Churaev, Johann Riemensberger, Paul Seidler, and Tobias J Kippenberger, “An ultra-broadband photonic-chip-based traveling-wave parametric amplifier,” arXiv preprint arXiv:2404.08609 (2024).
- [86] F. Mondain, T. Lunghi, A. Zavatta, E. Gouzien, F. Dautre, M. De Micheli, S. Tanzilli, and V. D’Auria, “Chip-based squeezing at a telecom wavelength,” *Photon. Res.* **7**, A36–A39 (2019).
- [87] Avik Dutt, Kevin Luke, Sasikanth Manipatruni, Alexander L. Gaeta, Paulo Nussenzevig, and Michal Lipson, “On-Chip Optical Squeezing,” *Physical Review Applied* **3**, 044005 (2015).
- [88] Hubert S. Stokowski, Timothy P. McKenna, Taewon Park, Alexander Y. Hwang, Devin J. Dean, Oguz Tolga Celik, Vahid Ansari, Martin M. Fejer, and Amir H. Safavi-Naeini, “Integrated quantum optical phase sensor in thin film lithium niobate,” *Nature Communications* **14**, 3355 (2023).
- [89] Yun Zhao, Yoshitomo Okawachi, Jae K. Jang, Xingchen

- Ji, Michal Lipson, and Alexander L. Gaeta, “Near-Degenerate Quadrature-Squeezed Vacuum Generation on a Silicon-Nitride Chip,” *Physical Review Letters* **124**, 193601 (2020).
- [90] Takahiro Kashiwazaki, Naoto Takanashi, Taichi Yamashima, Takushi Kazama, Koji Enbutsu, Ryoichi Kasahara, Takeshi Umeki, and Akira Furusawa, “Continuous-wave 6-dB-squeezed light with 2.5-THz-bandwidth from single-mode PPLN waveguide,” *APL Photonics* **5**, 036104 (2020).
- [91] Henning Vahlbruch, Moritz Mehmet, Karsten Danzmann, and Roman Schnabel, “Detection of 15 dB squeezed states of light and their application for the absolute calibration of photoelectric quantum efficiency,” *Physical Review Letters* **117**, 110801 (2016).
- [92] Igor Aharonovich and Elke Neu, “Diamond Nanophotonics,” *Advanced Optical Materials* **2**, 911–928 (2014).
- [93] D. Steinmetz, E. Neu, J. Meijer, W. Bolse, and C. Becher, “Single photon emitters based on Ni/Si related defects in single crystalline diamond,” *Applied Physics B* **102**, 451–458 (2011).
- [94] J. R. Rabeau, Y. L. Chin, S. Praver, F. Jelezko, T. Gaebel, and J. Wrachtrup, “Fabrication of single nickel-nitrogen defects in diamond by chemical vapor deposition,” *Applied Physics Letters* **86**, 131926 (2005).
- [95] T Gaebel, I Popa, A Gruber, M Domhan, F Jelezko, and J Wrachtrup, “Stable single-photon source in the near infrared,” *New Journal of Physics* **6**, 98 (2004).
- [96] E. Sörman, N. T. Son, W. M. Chen, O. Kordina, C. Hallin, and E. Janzén, “Silicon vacancy related defect in 4H and 6H SiC,” *Physical Review B* **61**, 2613–2620 (2000).
- [97] Nguyen T. Son, Christopher P. Anderson, Alexandre Bourassa, Kevin C. Miao, Charles Babin, Matthias Widmann, Matthias Niethammer, Jawad Ul Hassan, Naoya Morioka, Ivan G. Ivanov, Florian Kaiser, Joerg Wrachtrup, and David D. Awschalom, “Developing silicon carbide for quantum spintronics,” *Applied Physics Letters* **116**, 190501 (2020).
- [98] Daniel Franke, Daniel K. Harris, Ou Chen, Oliver T. Bruns, Jessica A. Carr, Mark W. B. Wilson, and Mounqi G. Bawendi, “Continuous injection synthesis of indium arsenide quantum dots emissive in the short-wavelength infrared,” *Nature Communications* **7**, 12749 (2016).
- [99] Ch. Heyn, A. Stemann, T. Köppen, Ch. Strelow, T. Kipp, M. Grave, S. Mendach, and W. Hansen, “Highly uniform and strain-free GaAs quantum dots fabricated by filling of self-assembled nanoholes,” *Applied Physics Letters* **94**, 183113 (2009).
- [100] Liang Zhai, Matthias C. Löbl, Giang N. Nguyen, Julian Ritzmann, Alisa Javadi, Clemens Spinnler, Andreas D. Wieck, Arne Ludwig, and Richard J. Warburton, “Low-noise GaAs quantum dots for quantum photonics,” *Nature Communications* **11**, 4745 (2020).
- [101] Zhengtao Deng, Olaf Schulz, Su Lin, Baoquan Ding, Xiaowei Liu, XiXi Wei, Robert Ros, Hao Yan, and Yan Liu, “Aqueous Synthesis of Zinc Blende CdTe/CdS Magic-Core/Thick-Shell Tetrahedral-Shaped Nanocrystals with Emission Tunable to Near-Infrared,” *Journal of the American Chemical Society* **132**, 5592–5593 (2010).
- [102] David Jurbergs, Elena Rogojina, Lorenzo Mangolini, and Uwe Kortshagen, “Silicon nanocrystals with ensemble quantum yields exceeding 60%,” *Applied Physics Letters* **88**, 233116 (2006).
- [103] Daniel A. Ruddy, Justin C. Johnson, E. Ryan Smith, and Nathan R. Neale, “Size and Bandgap Control in the Solution-Phase Synthesis of Near-Infrared-Emitting Germanium Nanocrystals,” *ACS Nano* **4**, 7459–7466 (2010).
- [104] Tom Feng and Bradley D. Schwartz, “Characteristics and origin of the 1.681 eV luminescence center in chemical-vapor-deposited diamond films,” *Journal of Applied Physics* **73**, 1415–1425 (1993).
- [105] Pao-Kang Chen, Ian Briggs, Chaohan Cui, Liang Zhang, Manav Shah, and Linran Fan, “Adapted poling to break the nonlinear efficiency limit in nanophotonic lithium niobate waveguides,” *Nature Nanotechnology* **19**, 44–50 (2024).